BES-manuscript

1 Introduction

Soils contain the largest reservoir of terrestrial carbon (Jobbágy and Jackson 2000). Accumulation of soil organic matter can be influenced by biotic factors from aboveground plant inputs (Jackson et al. 2017), which in turn are influenced through environmental factors such as growing season length, temperature, and moisture (Desai et al. 2022). These biotic factors provide natural climate-based solutions to offsetting any net increases of the terrestrial carbon cycle from greenhouse gas emissions (Friedlingstein et al. 2023).

Ecological networks such as the National Ecological Observatory Network (NEON) and others (e.g. FLUXNET or the Integrated Carbon Observation System) present a significant advancement in the nearly continuous observation of biogeochemical processes at the continental scale. Notably, at 47 core terrestrial sites across the continental United States NEON provides half-hourly measurements of soil carbon content, soil CO_2 concentration, temperature, and moisture at different vertical depths. In turn, FLUXNET provides measurements of the cumulative sum of all ecosystem carbon fluxes in an airshed using the eddy covariance technique (Baldocchi 2014). Soil observations from NEON data provided by NEON is on the same timescale and standardized with eddy covariance measurements from FLUXNET. When combined together NEON and FLUXNET data reconciling differences between model-derived or data-estimated components (Luo et al. 2011; Phillips et al. 2017; J. Shao et al. 2015; P. Shao et al. 2013; Sihi et al. 2016; Jian et al. 2022).

Beyond observations of soil CO_2 concentrations or other environmental variables such as moisture or temperature, a key quantity is soil carbon fluxes (Ben Bond-Lamberty et al. 2024). A soil carbon flux to the atmosphere (F_S, units μmol m^{-2} s^{-1}) represents the aggregate process of transfer of soil CO_2 to the atmosphere from physical and biological processes (e.g. diffusion and microbial and autotrophic respiration). Soil carbon fluxes can be coupled with empirical or process models of soil carbon. Soil carbon fluxes can be assumed to represent soil carbon respiration from autotrophic or heterotrophic sources (**davidson_variability_2006?**), typically assumed to be static across the soil biome and modeled with a exponential Q_{10} paradigm (**bond-lamberty_contribution_2004-1?**; **chen_does_2005?**; **hamdi_synthesis_2013?**).

Measurement of F_S is done through directly with soil chambers (e.g. LICOR or XXXX) or from soil measurements at different depths in the soil. In the latter case, the flux-gradient method is an approach derives from the mass conservation from the vertical soil depth z at steady state by applying Fick's law of diffusion. A simplifying assumption for the flux-gradient method is that there no mass transfer in the other spatial dimensions x and y (Maier and Schack-Kirchner 2014). The diffusivity profile across the soil depth is a function of soil temperature, soil volumetric water content, atmospheric air pressure, and soil bulk density (Millington and Shearer 1971; Moldrup et al. 1999).

A growing number of databases such as the Soil Respiration Database (SRDB) or Continuous Soil Respiration Database (COSORE) add to the growing network of observations of soil fluxes (Ben Bond-Lamberty et al. 2020; Jian et al. 2021; Jiang et al. 2024; B. Bond-Lamberty and Thomson 2010; Ben Bond-Lamberty 2018). Currently NEON provides all measurements to calculuate F_S from Fick's law, but it was descoped from the initial network launch (Berenbaum et al. 2015). Deriving data-based measurements of F_S is a high priority.

This study describes efforts to derive a standardized estimate of F_S at all terrestrial NEON sites. Derived values of F_S are then validated from a subset of field observations. Key objectives of this study are to:

- apply the flux-gradeint method to measurement to current NEON sites
- benchmark produced soil carbon fluxes to other ancillary measusrements (e.g. SRDB, measurements of soil respiration)
- identify sources of error for future work.

2 Materials and Methods

2.1 Study sites

We selected six terrestrial NEON sites for analysis. These sites span a range of environmental gradients and terrestrial domains for analysis (Table 1). Over the course of two field campaigns in 2022 and 2024 we conducted weekly visits at each site through selecting a specific in the soil sampling array, installing a temporary soil collar, and doing direct flux measurements. These data were then compared for analysis later.

Table 1: Listing of NEON sites studied for field work and analysis

Site	Location	Ecosystem type	Mean annual temperature (sampling)	Mean annual precipitation (sampling)
Santa Rita Experimental Range	31.91068, -110.83549	Shrubland	19.3°C	346.2 mm
San Joaquin Experimental Range	37.10878, -119.73228	Oak woodland	16.4°C	539.62 mm
Wind River Experimental Forest	45.82049, -121.95191	Evergreen forest	9.2°C	2225 mm
Chase Lake National Wildlife Refuge	47.1282, -99.241334	Restored prairie grassland	4.9°C	495 mm
Konza Prairie Biological Station	39.100774, -96.563075	Tallgrass Prairie	12.4°C	870 mm
University of Notre Dame Environmental Research Center	46.23391, -89.537254	Deciduous forest	4.3°C	802 mm

IDEA: Could have a sparkline plot of temperature / precip over the course of the time spent at each site, although admittedly we didn't see THAT much variation when sampling.

2.2 Field methods

In order to acquire field data to validate model predictions of flux, we conducted field measurement campaigns at the siz core terrestrial NEON sites listed above. SJER, SRER, and WREF were visited during May and June of 2022, and WOOD, KONZ, and UNDE during May and June of 2024. We spent a week at each site, taking daily measurements of flux on an hourly or half-hourly interval after letting soil collar(s) equilibrate for approximately 24 hours.

2.2.1 Soil collar placement

Either one (2022 sampling campaign) or two (2024 sampling campaign) PVC soil collars (FIXME: diameter) were installed in close proximity to the permanent NEON soil sensors at each site. The soil plot where measurements was taken was chosen at each site in consultation with NEON staff to maximize likelihood of quality soil sensor measurements during the duration of the IRGA measurements at each site.

IDEA: Add graphic of soil plot layout and placement of soil collar(s) – could make diagram in OmniGraffle?

2.2.2 Infrared gas analyzer measurements of soil CO_2 flux

During the summer 2022 field campaign, a LI-COR 6800 with soil flux chamber attachment was used to measure soil fluxes for 8 hours each day on an hourly interval. During the summer 2024 field campaign, the LI-6800 measurements were taken on a half-hourly interval and were paired with an automated soil flux chamber setup (FIXME multiplexer, IRGA, chamber model numbers) that made automated measurements on a half-hourly interval 24 hours a day while we were on site. Each instrument was paired with a soil temperature and moisture probe (FIXME: Stevens model #) that was used to make soil temperature and moisture measurements concurrent with the CO_2 flux measurements.

Dead bands, measurement duration, instrument self-testing.

2.2.3 Post-collection processing of data

LI-COR SoilFluxPro software to assess dead band and measurement duration.

2.3 neonSoilFlux R package

We developed an R package (`neonSoilFlux`; https://CRAN.R-project.org/package=neonSoilFlux) to compute half-hourly soil carbon fluxes and uncertainties from NEON data. The objective of the `neonSoilFlux` package is a unified workflow soil data acquisition and analysis that supplements existing data acquisition software through the `neonUtilities` R package (https://CRAN.R-project.org/package=neonUtilities). Figure 1 outlines the basic workflow of the package.

At a given NEON observation there are five different replicate soil sensor arrays, with each sampling at five different soil depths (Figure 2). The `neonSoilFlux` package acquires measured soil water content (National Ecological Observatory Network (NEON) 2024e), soil CO_2 concentration (National Ecological Observatory Network (NEON) 2024b), barometric pressure (National Ecological Observatory Network (NEON) 2024a), soil temperature (National Ecological Observatory Network (NEON) 2024d), and soil properties (e.g. bulk density) (National Ecological Observatory Network (NEON) 2024c). The static soil properties are periodically collected and assumed to be constant for the monthly observation period.

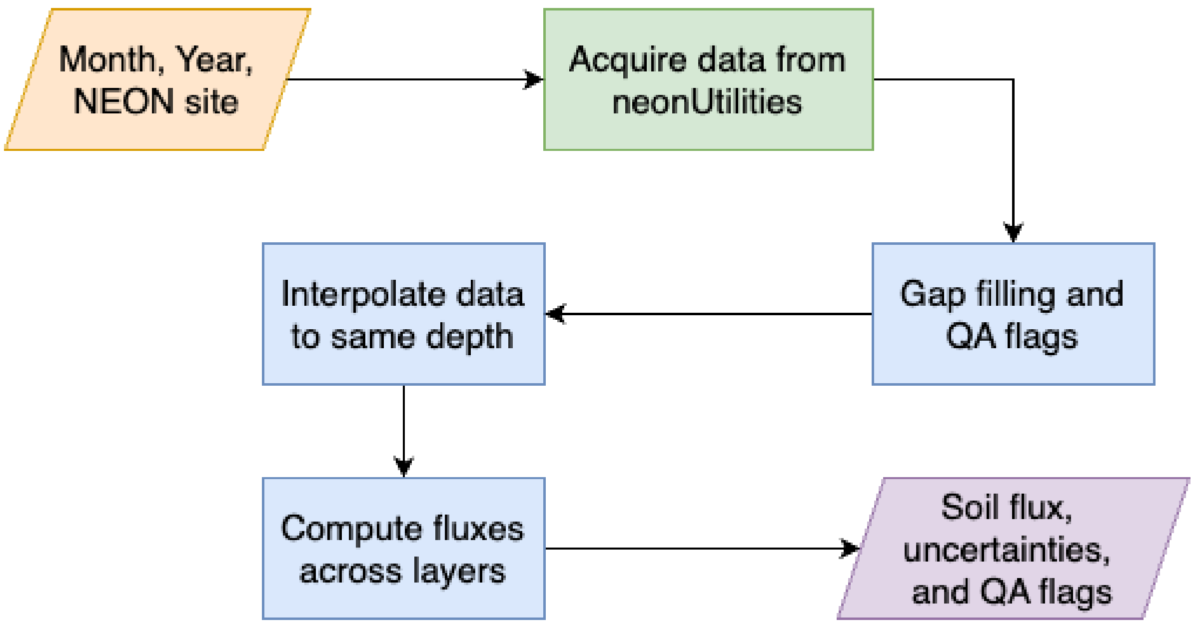

Figure 1: Diagram of `neonSoilFlux` R package. For a given month and NEON site, the package acquires all relevant data to compute F_S using the `neonUtilities` R package. Data are gap-filled according to reported QA flags and interpolated to the same measurement depth before computing the soil flux, uncertainties, and final QA flags.

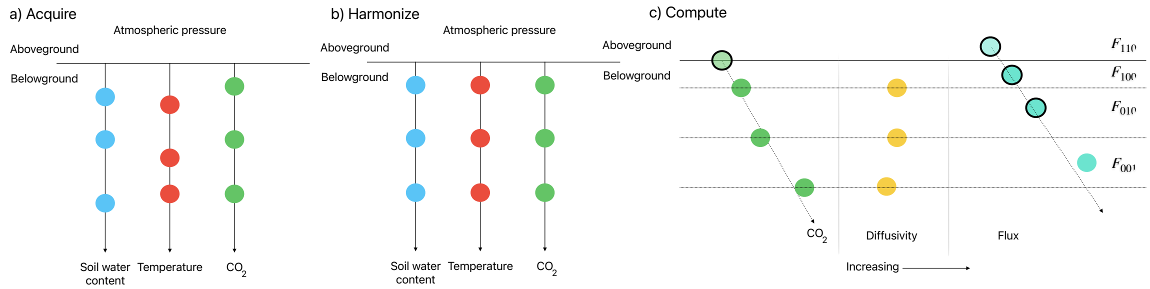

Figure 2: Model diagram for data workflow for the neonSoilFlux R package. a) Acquire: Data are obtained from given NEON location and horizontal sensor location, which includes soil water content, soil temperature, CO_2 concentration, and atmospheric pressure. All data are screened for quality assurance, with gap-filling of missing data reported. b) Any belowground data are then harmonized to the same depth as CO_2 concentrations using linear regression. c) The flux across a given depth is computed via Fick's law, denoted with F_{ijk}, where i, j, or k are either 0 or 1 denoting the layer the flux is computed across (i = closest to surface, k = deepest). The surface flux is all possible combinations of F_{ijk} extrapolating the flux measurements to the surface, so F_{110} is the surface flux intercept linearly extrapolating the measurements F_{010} and F_{100}.

The workflow to computing a value of F_S with the `neonSoilFlux` consists of three primary steps. First, NEON data are acquired for a given site and month via the `neonUtilities` R package (yellow parallelogram and green rectangle in Figure 1 and Panel a in Figure 2). Acquired environmental data can be exported to a comma separated value file for additional analysis. Quality assurance (QA) flags with an observation are reported as an indicator variable.

The next step is harmonizing the data to compute soil fluxes across soil layers. This step consists of three different actions (blue rectangles in Figure 1 and Panel b in Figure 2). If a given observation did is reported as not passing a quality assurance check we applied a gap filling method to replace that measurement with its monthly mean at that same depth (Section 2.3.1). Belowground measurements of soil water and soil temperature are then interpolated to the same depth as soil CO_2 measurements. The diffusivity (Section 2.3.2) and soil flux across different soil layers (Section 2.3.3) are then computed.

The final step is computing a surface soil flux through extrapolation to the surface (purple parallelogram in Figure 1 and Panel c in Figure 2). Uncertainty on a soil flux measurement is computed through quadrature. An aggregate QA flag for each environmental measurement is also reported, representing if any gap-filled measurements were used in the computation of a soil flux. Within the soil flux-gradient method, several different approaches can be used to derive a surface flux (Maier and Schack-Kirchner 2014); the `neonSoilFlux` package reports eight different possible values of soil surface flux (Section 2.3.3).

2.3.1 Gap-filling routine

NEON reports QA flags as a binary value for a given measurement and half-hourly time. We replaced any flagged measurements at a location's spatial depth z with a bootstrapped sample of the monthly mean for all un-flagged measurements for that month. hese measurements are represented by the vector $\mathbf{m}$, standard errors σ, and the 95% confidence interval (the so-called expanded uncertainty, Farrance and Frenkel (2012)) ϵ. All of these vectors have length M. We have that $\vec{\sigma}_i \leq \vec{\epsilon}_i$. We define the bias as $\mathbf{b} = \sqrt{\epsilon^2 - \sigma^2}$.

We generate a vector of bootstrap samples of the distribution of the monthly mean $\overline{m}$ and monthly standard error $\overline{\sigma}$ the following ways:

1. Randomly sample from the uncertainty and bias independently: σ_j and the bias $\mathbf{b}_k$ (not necessarily the same sample)
2. Generate a vector $\mathbf{n}$ of length N, where $\mathbf{n}_i$ is a random sample from a normal distribution with mean m_i and standard deviation σ_j. Since $M < N$, values from $\mathbf{m}$ will be reused.
3. With these N random samples, $\overline{y}_i = \overline{\vec{x}} + \vec{b}_k$ and s_i is the sample standard deviation of $\vec{x}$. We expect that $s_i \approx \vec{\sigma}_j$.
4. The reported monthly mean and standard deviation are then computed $\overline{\overline{y}}$ and $\overline{s}$. Measurements and uncertainties that did not pass the QA check are then substituted with $\overline{\overline{y}}$ and $\overline{s}$.

2.3.2 Diffusivity computation

Soil diffusivity D_a at a given measurement depth is the product of the diffusivity in free air $D_{a,0}$ (m^2 s^{-1}) and the tortuosity ξ (no units) (Millington and Shearer 1971). Surface barometric pressure (kPa) (National Ecological Observatory Network (NEON) 2024a), soil temperature at depth (National Ecological Observatory Network (NEON) 2024d), soil water content (National Ecological Observatory Network (NEON) 2024e), and soil physical properties (National Ecological Observatory Network (NEON) 2024c). Soil physical properties are surveyed once at each site, whereas the other measurements are provided on a half-hourly basis.

We compute $D_{a,0}$ with Equation 1:

$$D_{a,0} = 0.0000147 \cdot \left(\frac{T_i + 273.15}{293.15} \right)^{1.75} \cdot \left(\frac{P}{101.3} \right) \tag{1}$$

where T_i is soil temperature (°C) at depth i (National Ecological Observatory Network (NEON) 2024d) and P surface barometric pressure (kPa) (National Ecological Observatory Network

(NEON) 2024a). At that soil depth, the tortuosity ξ is defined by Equation 2 (Millington and Shearer 1971):

$$\xi = \frac{(\phi - SWC_i)^{10/3}}{\phi^2} \tag{2}$$

In Equation 2, SWC is the soil water content at depth i (National Ecological Observatory Network (NEON) 2024e) and ϕ is the porosity (Equation 3), which in turn is a function of soil physical properties (National Ecological Observatory Network (NEON) 2024c).

The tortuosity ξ is computed from soil porosity ϕ. :

$$\phi = \left(1 - \frac{\rho_s}{\rho_m}\right)(1 - f_V) \tag{3}$$

In Equation 3, ρ_m is the particle density of mineral soil (2.65 g cm^{-3}), ρ_s the soil bulk density (g cm^{-3}) excluding coarse fragments greater than 2 mm (National Ecological Observatory Network (NEON) 2024c). The term f_V is a site-specific value that accounts for the proportion of soil fragments between 2-20 mm. Soil fragments greater than 20 mm were not estimated due to limitations in the amount of soil that can be analyzed (National Ecological Observatory Network (NEON) 2024c). We assume there are no pores within rocks. Values of ρ_s, ρ_m are assumed to be constant across the soil profile and the same at each site sampling location.

2.3.3 Soil flux computation

We applied Fick's law (Equation 4) to compute the soil flux F_{ij} (μmol m^{-2} s^{-1}) across two adjacent soil depths i and j:

$$F_{ij} = -D_a \frac{dC}{dz} \tag{4}$$

where D_a is the diffusivity (m^2 s^{-1}) and $\frac{dC}{dz}$ is the gradient of CO_2 molar concentration (μmol m^{-3}, so the gradient has units of μmol m^{-3} m^{-1}). The diffusivity (described below) is a function of soil temperature, soil water content, and soil physical properties. The soil surface flux is theoretically defined by applying Equation 4 to measurements collected at the soil surface and directly below the surface. Measurements of soil temperature, soil water content, and soil CO_2 molar concentration across the soil profile allow for application of Equation **??** across different soil depths. The flux gradient method approximates the soil surface flux either by (1) extrapolation of Equation 4 across sub-surface measurement depths to the surface, typically assuming soil flux is a linear function of depth (Maier and Schack-Kirchner 2014) or (2) linear extrapolation of D_a to the surface and from direct calculation of $\frac{dC}{dz}$ from the CO_2 profile. All these approaches are pThe `neonSoilFlux` package provides several different methods to compute F_s for the end-user to compare.

2.3.4 Reporting of surface fluxes

A surface flux estimate is derived from Fick's Law (Equation 4), which is the product of a diffusivity and a CO_2 concentration gradient (Maier and Schack-Kirchner 2014). The `neonSoilFlux` package provides eight different surface flux estimates, which represent different considerations of how Fick's Law is applied. First, we apply simple linear regression to both CO_2 and D_a at the three different measurement depths. Next, the slope and intercept (and uncertainty by quadrature) from these regressions are used to compute a suite of eight different surface flux estimates (denoted by F_{ijk}):

- F_{000} is a surface flux estimate using the intercept of the linear regression of D_a and the slope from linear regression of CO_2 (which represents $\frac{dC}{dz}$ in Fick's Law). Tang et al. (2003) used this approach to compute fluxes in an oak-grass savannah.
- F_{010}, F_{001} are fluxes across the two most shallow layers and two deepest layers respectively. The diffusivity used in Fick's Law is always at the deeper measurement layer. When used as a surface flux estimate we assume CO_2 remains constant above this flux depth.
- F_{100} is a flux estimate where the gradient $\frac{dC}{dz}$ is estimated using the intercept from linear regression of CO_2 and the top measurement depth for CO_2. The diffusivity used in Fick's Law is always at the first measurement layer. de Jong and Schappert (1972) applied this approach in a Canadian prairie.
- F_{110}, F_{101}, F_{011} are a surface flux estimates using linear extrapolation between F_{100} and F_{010}; F_{100} and F_{001}; or F_010 and F_{001} respectively. Hirano, Kim, and Tanaka (2003) and Tang et al. (2005) used an approach similar to F_{101} in a temperate deciduous broadleaf forest and ponderosa pine forest respectively.
- F_{111} is a surface flux estimate using linear extrapolation between F_{100}, F_{010}, and F_{001}.

Uncertainty in all F_{ijk} is computed through quadrature.

3 Results

Figure: flux results at the different levels (000,111,001,010,100) Diffusivity at the different levels for comparison (also include derived diffusivity?) Stats at the different levels (with the lags)

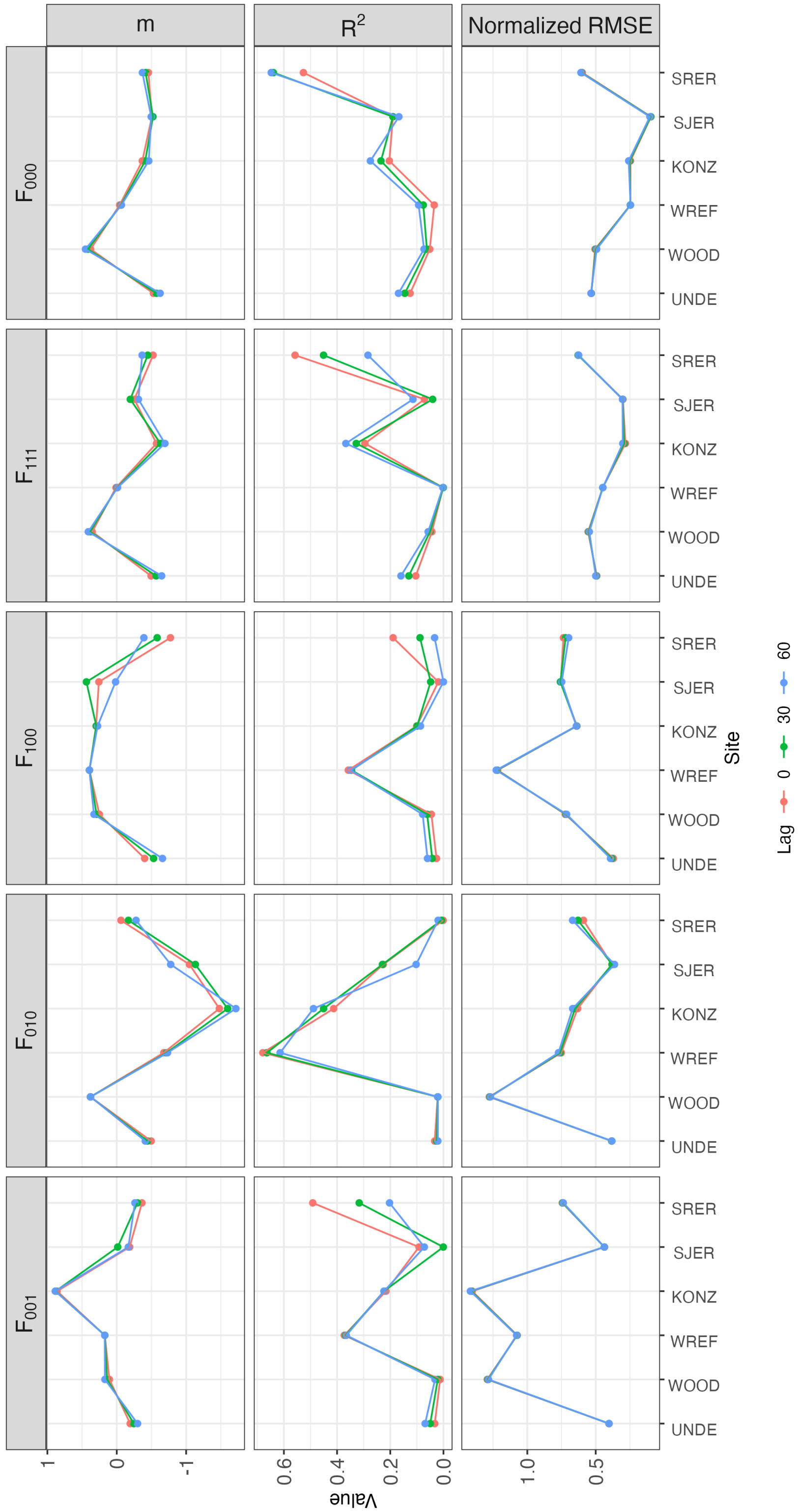
m
R2
Normalized RMSE
F000
F111
F100
F010
F001
SRER
SJER
KONZ
WREF
WOOD
UNDE
Site
Value
Lag
0
30
60

Figure 3

3.1 Field Data Measurements

3.1.1 LICOR 6800 results

3.1.2 LICOR 8250 results

3.2 Model Results

Results for the different flux computations Figure 4

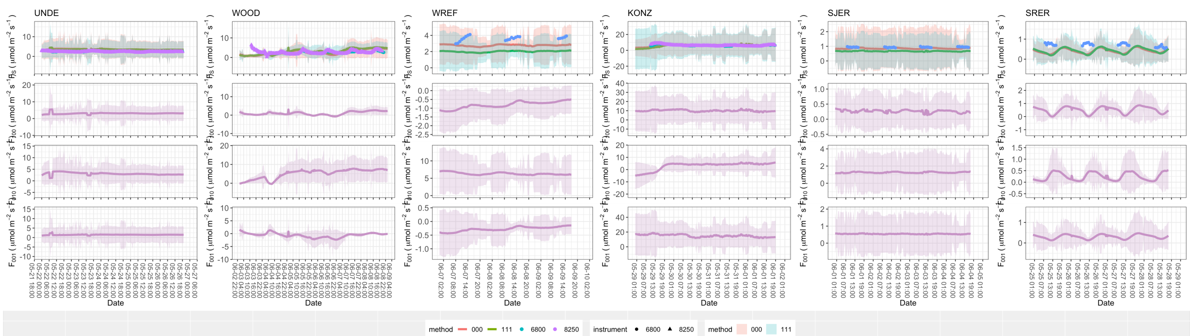

Figure 4: Results for different flux computations, organized by site (in increasing temperature show at each site) across different measurement levels. F_{000} comes from the diffusivity extrapolation and F_{111} extrapolation across the surface. Field measurements are shown at the top of each plot. The computed flux values are shown with reported uncertainty as well.

We evaluate the efficacy of results from the flux-gradient method in two ways. First, we calculated the signal to noise ratio (SNR), defined as the ratio of the reported flux to its uncertainty (F_{ijk}/σ_{ijk}).

We evaluated if the measured field fluxes were within the calculated uncertainty from the flux-gradient method using the various approaches outlined above. We observed that the calculated quadrature uncertainty in many cases can be much larger than the reported measurement (as shown through the signal to noise ratio, $\mathrm{SNR} = F_{ijk}/\sigma_{ijk}$. We evaluated $|F_S - F_{ijk}| < (1-\epsilon)\sigma_{ijk}$, where F_S is a measured field soil flux (LICOR 6800 or LICOR 8250) and F_{ijk} is a computed flux method from the flux-gradient, and σ_{ijk} is the reported uncertainty for the flux method. The parameter ϵ was an uncertainty reduction factor to evaluate how sensitive the results were given, measured by the proportion of field measurements contained in that range. These results are reported in Figure 5.

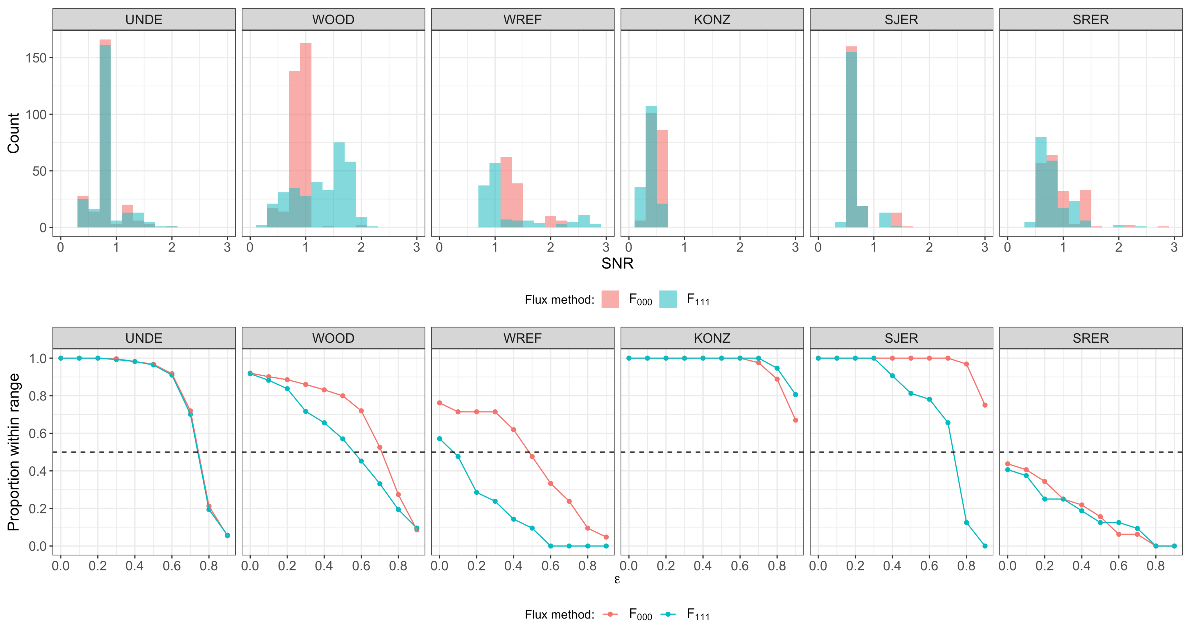

Figure 5: Top panel: distribution of SNR values across each of the different sites for the F_{000} and F_{111} flux gradient calculations. Bottom panel: Computation of uncertainty reduction to evaluate. As ϵ increases this indicates that the uncertainty estimate reduces, making it harder to be within the range. BLAH

4 Discussion

- CO_2 concentration and flux
- Temperature and moisture controls on respiration
- Evaluation of methods to estimate soil respiration
- Uncertainty reduction and what is the "correct" answer

5 Conclusions

6 Acknowledgments

7 Conflict of Interest Statements

Author Contributions

Baldocchi, Dennis. 2014. "Measuring Fluxes of Trace Gases and Energy Between Ecosystems and the Atmosphere - the State and Future of the Eddy Covariance Method." *Global Change Biology* 20 (12): 3600–3609. https://doi.org/10.1111/gcb.12649.

Berenbaum, May R, Stephen R Carpenter, Stephanie E Hampton, Steven W Running, and Dan C Stanzione. 2015. "Report from the NSF BIO Advisory Committee Subcommittee on NEON Scope Impacts."

Bond-Lamberty, Ben. 2018. "New Techniques and Data for Understanding the Global Soil Respiration Flux." *Earth's Future* 6 (9): 1176–80. https://doi.org/10.1029/2018EF000866.

Bond-Lamberty, Ben, Ashley Ballantyne, Erin Berryman, Etienne Fluet-Chouinard, Jinshi Jian, Kendalynn A. Morris, Ana Rey, and Rodrigo Vargas. 2024. "Twenty Years of Progress, Challenges, and Opportunities in Measuring and Understanding Soil Respiration." *Journal of Geophysical Research: Biogeosciences* 129 (2): e2023JG007637. https://doi.org/10.1029/2023JG007637.

Bond-Lamberty, Ben, Danielle S. Christianson, Avni Malhotra, Stephanie C. Pennington, Debjani Sihi, Amir AghaKouchak, Hassan Anjileli, et al. 2020. "COSORE: A Community Database for Continuous Soil Respiration and Other Soil-Atmosphere Greenhouse Gas Flux Data." *Global Change Biology* 26 (12): 7268–83. https://doi.org/10.1111/gcb.15353.

Bond-Lamberty, B., and A. Thomson. 2010. "A Global Database of Soil Respiration Data." *Biogeosciences* 7 (6): 1915–26. https://doi.org/10.5194/bg-7-1915-2010.

de Jong, E., and H. J. V. Schappert. 1972. "Calculation of Soil Respiration and Activity from CO_2 Profiles in the Soil." *Soil Science* 113 (5): 328–33.

Desai, Ankur R., Bailey A. Murphy, Susanne Wiesner, Jonathan Thom, Brian J. Butterworth, Nikaan Koupaei-Abyazani, Andi Muttaqin, et al. 2022. "Drivers of Decadal Carbon Fluxes

Across Temperate Ecosystems." *Journal of Geophysical Research: Biogeosciences* 127 (12): e2022JG007014. https://doi.org/10.1029/2022JG007014.

Farrance, Ian, and Robert Frenkel. 2012. "Uncertainty of Measurement: A Review of the Rules for Calculating Uncertainty Components Through Functional Relationships." *The Clinical Biochemist Reviews* 33 (2): 49–75.

Friedlingstein, Pierre, Michael O'Sullivan, Matthew W. Jones, Robbie M. Andrew, Dorothee C. E. Bakker, Judith Hauck, Peter Landschützer, et al. 2023. "Global Carbon Budget 2023." *Earth System Science Data* 15 (12): 5301–69. https://doi.org/10.5194/essd-15-5301-2023.

Hirano, Takashi, Honghyun Kim, and Yumiko Tanaka. 2003. "Long-Term Half-Hourly Measurement of Soil CO2 Concentration and Soil Respiration in a Temperate Deciduous Forest." *Journal of Geophysical Research: Atmospheres* 108 (D20). https://doi.org/10.1029/2003JD003766.

Jackson, Robert B., Kate Lajtha, Susan E. Crow, Gustaf Hugelius, Marc G. Kramer, and Gervasio Piñeiro. 2017. "The Ecology of Soil Carbon: Pools, Vulnerabilities, and Biotic and Abiotic Controls." *Annual Review of Ecology, Evolution and Systematics* 48 (Volume 48, 2017): 419–45. https://doi.org/10.1146/annurev-ecolsys-112414-054234.

Jian, Jinshi, Vanessa Bailey, Kalyn Dorheim, Alexandra G. Konings, Dalei Hao, Alexey N. Shiklomanov, Abigail Snyder, et al. 2022. "Historically Inconsistent Productivity and Respiration Fluxes in the Global Terrestrial Carbon Cycle." *Nature Communications* 13 (1): 1733. https://doi.org/10.1038/s41467-022-29391-5.

Jian, Jinshi, Rodrigo Vargas, Kristina Anderson-Teixeira, Emma Stell, Valentine Herrmann, Mercedes Horn, Nazar Kholod, et al. 2021. "A Restructured and Updated Global Soil Respiration Database (SRDB-V5)." *Earth System Science Data* 13 (2): 255–67. https://doi.org/10.5194/essd-13-255-2021.

Jiang, Junjie, Lingxia Feng, Junguo Hu, Haoqi Liu, Chao Zhu, Baitong Chen, and Taolue Chen. 2024. "Global Soil Respiration Predictions with Associated Uncertainties from Different Spatio-Temporal Data Subsets." *Ecological Informatics* 82 (September): 102777. https://doi.org/10.1016/j.ecoinf.2024.102777.

Jobbágy, Esteban G., and Robert B. Jackson. 2000. "The Vertical Distribution of Soil Organic Carbon and Its Relation to Climate and Vegetation." *Ecological Applications* 10 (2): 423–36. https://doi.org/10.1890/1051-0761(2000)010%5B0423:TVDOSO%5D2.0.CO;2.

Luo, Yiqi, Kiona Ogle, Colin Tucker, Shenfeng Fei, Chao Gao, Shannon LaDeau, James S. Clark, and David S. Schimel. 2011. "Ecological Forecasting and Data Assimilation in a Data-Rich Era." *Ecological Applications* 21 (5): 1429–42. https://doi.org/10.1890/09-1275.1.

Maier, M., and H. Schack-Kirchner. 2014. "Using the Gradient Method to Determine Soil Gas Flux: A Review." *Agricultural and Forest Meteorology* 192–193 (July): 78–95. https://doi.org/10.1016/j.agrformet.2014.03.006.

Millington, R. J., and R. C. Shearer. 1971. "Diffusion in Aggregated Porous Media." *Soil Science* 111 (6): 372–78.

Moldrup, P., T. Olesen, T. Yamaguchi, P. Schjønning, and D. E. Rolston. 1999. "Modeling Diffusion and Reaction in Soils: 9. The Buckingham-Burdine-Campbell Equation for Gas Diffusivity in Undisturbed Soil." *Soil Science* 164 (2): 75.

National Ecological Observatory Network (NEON). 2024a. "Barometric Pressure (DP1.00004.001)." National Ecological Observatory Network (NEON). https://doi.org/10.48443/RT4V-KZ04.

———. 2024b. "Soil CO2 Concentration (DP1.00095.001)." National Ecological Observatory Network (NEON). https://doi.org/10.48443/E7GR-6G94.

———. 2024c. "Soil Physical and Chemical Properties, Megapit (DP1.00096.001)." National Ecological Observatory Network (NEON). https://doi.org/10.48443/S6ND-Q840.

———. 2024d. "Soil Temperature (DP1.00041.001)." National Ecological Observatory Network (NEON). https://doi.org/10.48443/Q24X-PW21.

———. 2024e. "Soil Water Content and Water Salinity (DP1.00094.001)." National Ecological Observatory Network (NEON). https://doi.org/10.48443/A8VY-Y813.

Phillips, Claire L., Ben Bond-Lamberty, Ankur R. Desai, Martin Lavoie, Dave Risk, Jianwu Tang, Katherine Todd-Brown, and Rodrigo Vargas. 2017. "The Value of Soil Respiration Measurements for Interpreting and Modeling Terrestrial Carbon Cycling." *Plant and Soil* 413 (1): 1–25. https://doi.org/10.1007/s11104-016-3084-x.

Shao, Junjiong, Xuhui Zhou, Yiqi Luo, Bo Li, Mika Aurela, David Billesbach, Peter D. Blanken, et al. 2015. "Biotic and Climatic Controls on Interannual Variability in Carbon Fluxes Across Terrestrial Ecosystems." *Agricultural and Forest Meteorology* 205 (June): 11–22. https://doi.org/10.1016/j.agrformet.2015.02.007.

Shao, Pu, Xubin Zeng, David J. P. Moore, and Xiaodong Zeng. 2013. "Soil Microbial Respiration from Observations and Earth System Models." *Environmental Research Letters* 8 (3): 034034. https://doi.org/10.1088/1748-9326/8/3/034034.

Sihi, Debjani, Stefan Gerber, Patrick W. Inglett, and Kanika Sharma Inglett. 2016. "Comparing Models of Microbial–Substrate Interactions and Their Response to Warming." *Biogeosciences* 13 (6): 1733–52. https://doi.org/10.5194/bg-13-1733-2016.

Tang, Jianwu, Dennis D Baldocchi, Ye Qi, and Liukang Xu. 2003. "Assessing Soil CO2 Efflux Using Continuous Measurements of CO2 Profiles in Soils with Small Solid-State Sensors." *Agricultural and Forest Meteorology* 118 (3): 207–20. https://doi.org/10.1016/S0168-1923(03)00112-6.

Tang, Jianwu, Laurent Misson, Alexander Gershenson, Weixin Cheng, and Allen H. Goldstein. 2005. "Continuous Measurements of Soil Respiration with and Without Roots in a Ponderosa Pine Plantation in the Sierra Nevada Mountains." *Agricultural and Forest Meteorology* 132 (3): 212–27. https://doi.org/10.1016/j.agrformet.2005.07.011.